© 2021. Published by The Company of Biologists Ltd | Journal of Cell Science (2021) 134, jcs257006. doi:10.1242/jcs.257006

RESEARCH ARTICLE

Intercellular and intracellular cilia orientation is coordinated by CELSR1 and CAMSAP3 in oviduct multi-ciliated cells

Fumiko Matsukawa Usami[1,2], Masaki Arata[1,3], Dongbo Shi[1,*], Sanae Oka[1], Yoko Higuchi[1], Fadel Tissir[4], Masatoshi Takeichi[5] and Toshihiko Fujimori[1,2,‡]

ABSTRACT

The molecular mechanisms by which cilia orientation is coordinated within and between multi-ciliated cells (MCCs) are not fully understood. In the mouse oviduct, MCCs exhibit a characteristic basal body (BB) orientation and microtubule gradient along the tissue axis. The intracellular polarities were moderately maintained in cells lacking CELSR1 (cadherin EGF LAG seven-pass G-type receptor 1), a planar cell polarity (PCP) factor involved in tissue polarity regulation, although the intercellular coordination of the polarities was disrupted. However, CAMSAP3 (calmodulin-regulated spectrin-associated protein 3), a microtubule minus-end regulator, was found to be critical for determining the intracellular BB orientation. CAMSAP3 localized to the base of cilia in a polarized manner, and its mutation led to the disruption of intracellular coordination of BB orientation, as well as the assembly of microtubules interconnecting BBs, without affecting PCP factor localization. Thus, both CELSR1 and CAMSAP3 are responsible for BB orientation but in distinct ways; their cooperation should therefore be critical for generating functional multi-ciliated tissues.

KEY WORDS: Basal body, Cytoskeleton, Oviduct, Planar cell polarity, Reproduction, Super-resolution microscopy

INTRODUCTION

Multi-ciliated cells (MCCs), which have a few hundred cilia on their apical surface (Brooks and Wallingford, 2014; Meunier and Azimzadeh, 2016; Reiter and Leroux, 2017; Spassky and Meunier, 2017; Boutin and Kodjabachian, 2019), are specialized cells found in the epithelium of the oviduct, the trachea and the ependyma of the brain. In the infundibulum of the mouse oviduct (fallopian tube), eggs released from the ovaries are transported to the uterine side by the movement of multi-cilia (Shi et al., 2011; Li and Winuthayanon, 2016). In MCCs, the direction of cilia movement is coordinated both intracellularly (within each cell: rotational polarity) and intercellularly (between cells: tissue-level polarity) along the axis of the organ to generate directed flow (Hirota et al., 2010; Guirao et al., 2010; Mirzadeh et al., 2010; Tissir et al., 2010; Boutin et al., 2014; Meunier and Azimzadeh, 2016). Ciliary abnormalities, including motility and polarity as well as ciliogenesis in various organs, can lead to various disorders (Choksi et al., 2014; Reiter and Leroux, 2017).

This unidirectional ciliary movement is reinforced by the structural polarity of each cilium. The basal body (BB) found at the base of the cilium has similar components to the centriole and supports the axoneme in the apical cytoplasm. The basal foot (BF) is an electron-dense structure that projects unidirectionally from the BB (Werner et al., 2011; Kunimoto et al., 2012; Reiter et al., 2012; Clare et al., 2014; Garcia and Reiter, 2016) in the same orientation as the effective stroke of the cilium.

The orientation of multiple cilia reflects the polarity of each cell. In epithelial cells, in addition to apicobasal polarity, planar cell polarity (PCP) runs perpendicular to the apicobasal plane within the plane of the epithelium (Aw and Devenport, 2017; Butler and Wallingford, 2017; Henderson et al., 2018). PCP factors, which include CELSR1 (cadherin EGF LAG seven-pass G-type receptor 1) and the Van Gogh-like proteins VANGL1 and VANGL2 are proteins involved in regulating PCP that were initially identified by genetic screens performed in *Drosophila melanogaster*; many are conserved in vertebrates regulating morphological polarities extending over multiple cells (Boutin et al., 2012; Shi et al., 2013; Devenport, 2014; Hale and Strutt, 2015; Yang and Mlodzik, 2015; Koyama et al., 2016; Shi et al., 2016a; Butler and Wallingford, 2017; Koyama et al., 2019). These factors localize asymmetrically at cell boundaries in each cell according to the tissue's polarity (Park et al., 2008; Mitchell et al., 2009; Hirota et al., 2010; Ohata et al., 2014). A cytoplasmic PCP factor, DVL2 (dishevelled2), also localizes to the base of cilia, in addition to cell boundaries in *Xenopus laevis* epidermis and mouse ependyma. PCP factors are essential for regulating cilia polarity in *Xenopus* epidermis (Park et al., 2008; Mitchell et al., 2009), mouse ventricular ependymal cells (Guirao et al., 2010; Hirota et al., 2010; Mirzadeh et al., 2010; Tissir et al., 2010; Boutin et al., 2014; Ohata et al., 2014; Takagishi et al., 2017, 2020), mouse trachea (Vladar et al., 2012) and mouse oviduct (Shi et al., 2014). We previously reported that *Celsr1*-deficient females are sterile because of multiple PCP defects in the mutant oviducts (Shi et al., 2014). By using fluid flow analysis and direct observation of ciliary movement, we found that the directions in which the cilia of MCCs move were not aligned along the longitudinal axis of the oviduct. Our analysis following electron microscopy observation has revealed that cilia orientation is not coordinated in *Celsr1*$^{-/-}$ mutant oviducts. However, we could only observe details in a very limited area, and could not simultaneously determine BB orientation across multiple cells.

[1]Division of Embryology, National Institute for Basic Biology, 5-1 Higashiyama, Myodaiji-cho, Okazaki, 444-8787 Japan. [2]Department of Basic Biology, School of Life Science, SOKENDAI, The Graduate University for Advanced Studies, 5-1 Higashiyama, Myodaiji-cho, Okazaki, 444-8787 Japan. [3]Graduate School of Science, Nagoya University, Nagoya, 464-8601 Japan. [4]Université Catholique de Louvain, Institute of Neuroscience, Developmental Neurobiology Unit, Avenue Mounier 73, Box B1.73.16, Brussels 1200, Belgium. [5]Laboratory for Cell Adhesion and Tissue Patterning, RIKEN Center for Biosystems Dynamics Research, 2-2-3 Minatojima-Minamimachi, Chuo-ku, Kobe 650-0047, Japan.
*Present address: Center for Organismal Studies Heidelberg, Im Neuenheimer Feld 230, 69120 Heidelberg, Germany.

‡Author for correspondence (fujimori@nibb.ac.jp)

F.M.U., 0000-0002-4423-1789; M.A., 0000-0001-5229-1346; D.S., 0000-0002-4408-3042; S.O., 0000-0002-2786-6635; Y.H., 0000-0001-6066-8190; F.T., 0000-0002-9292-6622; M.T., 0000-0002-9931-3378; T.F., 0000-0001-5200-4634

Handling Editor: David Stephens
Received 7 November 2020; Accepted 4 January 2021

Journal of Cell Science (2021) 134, jcs257006. doi:10.1242/jcs.257006

Cytoskeletal elements, namely microtubules, intermediate filaments and actin filaments, are connected to the BB (Sandoz et al., 1988; Werner et al., 2011; Clare et al., 2014; Antoniades et al., 2014; Chevalier et al., 2015; Herawati et al., 2016; Tateishi et al., 2017) and supposedly provide mechanical support for cilia. The mechanism by which these cytoskeletal elements are involved in cilia polarity regulation differs between animal species and between organs (Iftode and Fleury-Aubusson, 2003; Werner et al., 2011; Antoniades et al., 2014; Bayless et al., 2019; Soh et al., 2019). In mouse trachea, actin filaments function in BB docking to the apical surface of cells, and microtubules regulate cilia orientation (Herawati et al., 2016). Electron microscopy has revealed that microtubules accumulate near the tip of the BF in various animal species (Reed et al., 1984; Sandoz et al., 1988; Lemullois and Marty, 1990). In addition, microtubules are concentrated at the apical cell–cell boundary in a polarized manner in MCCs of mouse ependyma and trachea; this polarized enrichment correlates with the orientation of BBs (Vladar et al., 2012; Boutin et al., 2014; Herawati et al., 2016; Takagishi et al., 2017). We have also previously shown that EB1, which localizes to the plus-end of microtubules, is enriched in a polarized manner in mouse oviduct MCCs (Shi et al., 2016b). The molecular mechanisms underlying microtubule control of cilia orientation remain unclear.

In this study, we explored how the orientation of cilia is coordinated within each cell and between cells, focusing on MCCs in the infundibulum of the mouse oviduct. To this end, we made use of super-resolution microscopy, stimulated emission depletion microscopy (STED), to dissect the roles of PCP factors and microtubules in establishing tissue-wide coordination of cilia orientation. In addition to the role of CELSR1, a PCP factor that organizes the orientation of cilia and polarity of microtubule enrichment at the tissue level, we found that CAMSAP3 [calmodulin-regulated spectrin-associated protein 3; also known as nezha (Meng et al., 2008)], a microtubule minus end-binding protein, localizes to BBs in a polarized manner, controls rotational polarity of cilia and organizes the assembly of microtubules interconnecting BBs.

RESULTS

Intracellular basal body orientation is moderately coordinated in *Celsr1*-deficient oviduct MCCs

To investigate the orientation of individual cilia across an epithelial sheet, we used super-resolution microscopy (STED). Oviducts of adult animals (11 weeks) were stained with anti-ODF2 antibody (Tateishi et al., 2013), a BB (distal and subdistal appendage) marker, and anti-centriolin antibody (Mazo et al., 2016), a BF marker. ODF2 formed a ring with an approximate diameter of 280 nm, and centriolin was detected as an ellipse with a major axis of about 160 nm, or as two adjacent puncta (Fig. 1A). The orientation of each BB was determined by the relative positions of ODF2 and centriolin (Fig. 1A′,A″). The average number of BBs in adult wild-type (WT) MCC was 201 per cell (n=20 cells, s.d.=25.7). We determined the orientation of 183 BBs in each cell on average (n=20 cells; Fig. 1B,C), choosing those with clear ODF2 and centriolin signals. The variation in BB orientation within each cell is indicated as cellular circular variance (CV) (Fig. 1D) (Shi et al., 2014), where cells with lower CV represent uniform BB orientation. Centriolin signals were localized to the uterine side of the ODF2 ring (Fig. 1B), indicating that BBs were regularly oriented in the same direction in each cell. The CVs were less than 0.2 (median=0.098) in all cells, suggesting uniform cilia orientation in WT cells. We also calculated the cellular mean BB orientation in each cell (Fig. 1C) and compared this value between adjacent cells (Fig. 1E). The mean BB orientation was also uniform between cells heading to the uterine side in the WT.

In the *Celsr1*$^{-/-}$ mutant, both ODF2 and centriolin signals were detected in each BB with the same shape and in the same relative positions as in WT. The average number of BBs in adult *Celsr1*$^{-/-}$ mutant cells was 199 per cell (n=20 cells, s.d.=27.7), which was comparable to WT. The number of BBs for which we could analyse the orientation was less in the *Celsr1*$^{-/-}$ mutant cells (127 BBs per cell on average; n=20 cells; Fig. 1B′,C′) than in WT, because the apical surface was not flat but dome shaped, and it was not easy to capture the orientation of cilia over a wide area in individual cells. The variation in BB orientation within each *Celsr1*$^{-/-}$ mutant cell was compared with WT. The CV values for the *Celsr1*$^{-/-}$ mutants were between 0.09 and 0.5 (median=0.23), which was significantly higher than WT, but still lower than completely random (Fig. 1D; Fig. S5). In the *Celsr1*$^{-/-}$ mutant, the mean BB orientation varied between cells. This was the case even when BB orientation was approximately aligned with lower CV values in neighboring cells (Fig. 1E′, purple and blue arrows).

These analyses confirmed that BBs in each cell are not randomly oriented in WT, and *Celsr1*$^{-/-}$ mutants show reduced coordinated orientation of BBs, and the mean BB orientation differed between cells. These results are consistent with our previous finding (Shi et al., 2014) and suggest that CELSR1 is involved in coordinating cilia orientation between cells, although other unidentified mechanisms appear to exist for aligning cilia orientation in each cell, even when CELSR1 is absent.

Polarized microtubule enrichment at the cell–cell boundary correlates with BB orientation in each cell even in the absence of CELSR1

We then examined the relationship between the organization of microtubules and BB orientation in oviduct MCCs of WT and *Celsr1*$^{-/-}$. In the WT, microtubules visualized by anti-β-tubulin antibody staining were asymmetrically enriched on the uterine side of the cell–cell boundary in each MCC (Fig. 2A). Moreover, a gradient of signals to this enrichment was observed near the apical surface (Fig. 2A; Fig. S1A). Quantitative analyses clearly indicated microtubule enrichment on the uterine side of MCCs in WT (Fig. 2B). In contrast, in the *Celsr1*$^{-/-}$ mutant, asymmetric enrichment of microtubules was evident in more than 75% of MCCs, but the direction of microtubule enrichment did not match between cells, nor did it match either the ovarian–uterine axis or fold morphology (Fig. 2A′, arrows, B′; Fig. S1D).

We next analysed the relationship between the orientation of microtubule enrichment and BB orientation in *Celsr1*$^{-/-}$. BB orientation was determined by ODF2 and centriolin signals as shown in Fig. 1. As the optimal fixation conditions for the anti-β-tubulin antibody and the anti-ODF2 and anti-centriolin antibodies are different, the respective staining signals were slightly different from that which is described above (Fig. 1A; Fig. 2A′). The β-tubulin signal was observed in the form of fine dots, nevertheless allowing us to observe its density gradient (Fig. 2C). The BB orientation was determined and quantified in cells where microtubule enrichment was observed (Fig. 2C′). These cells showed CV values lower than 0.25 (median=0.14), and the mean BB orientation (purple arrow in Fig. 2C′) in each cell coincided with the microtubule enrichment direction (yellow arrow in Fig. 2C; n=5 cells, average 210 BBs per cell).

Thus, microtubules were enriched near the apical surface of MCCs even in the absence of CELSR1, and the orientation of microtubule enrichment correlated with the mean BB orientation in each cell; however, microtubule enrichment orientation between cells was not aligned. These results indicate that BBs are oriented

Journal of Cell Science (2021) 134, jcs257006. doi:10.1242/jcs.257006

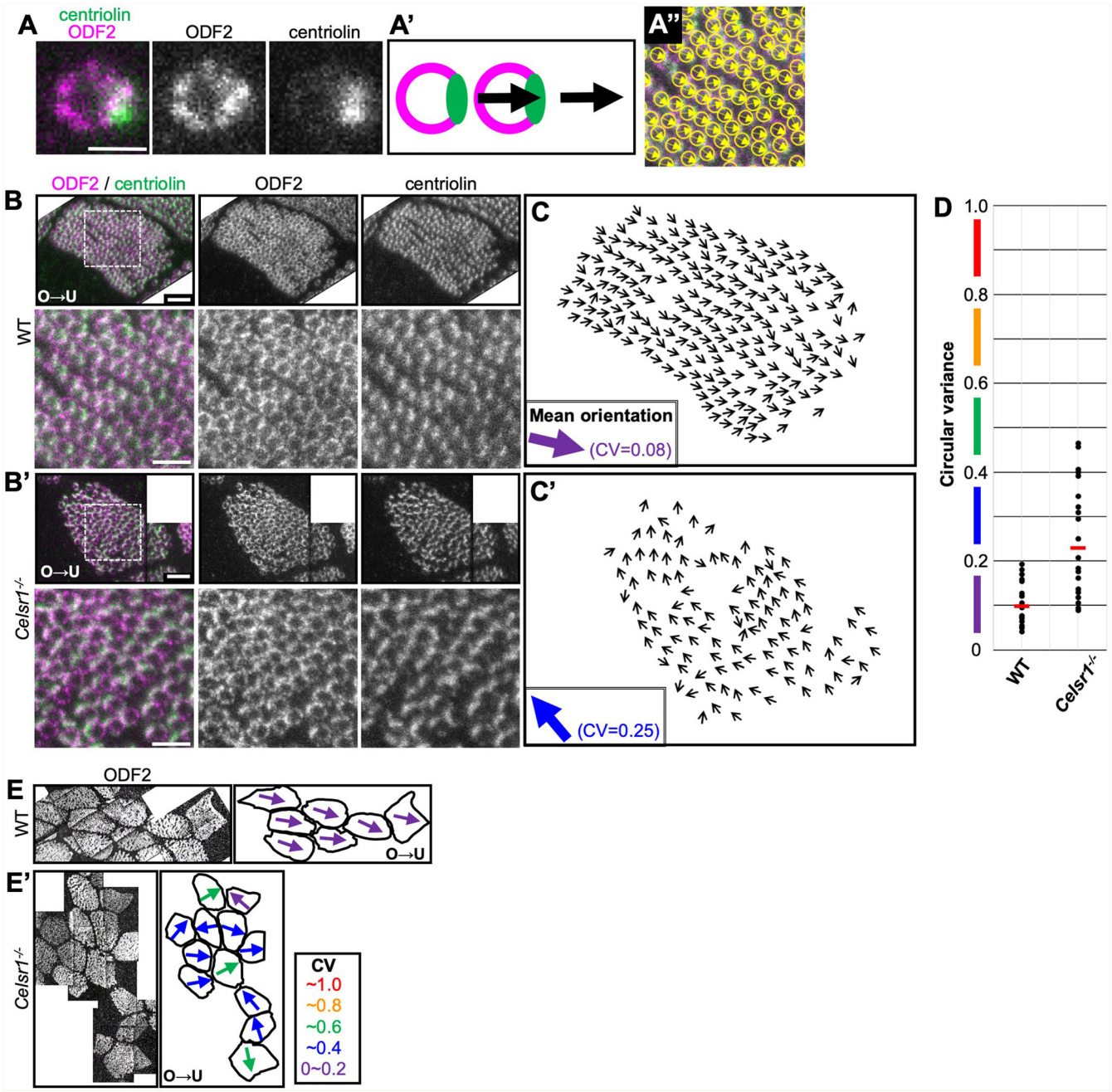

Fig. 1. Basal body orientation in *Celsr1*-deficient oviduct multi-ciliated cells. (A) Super-resolution microscope (STED) image of a basal body (BB) of wild-type (WT) oviduct MCCs after staining with anti-ODF2 (magenta) and anti-centriolin (green) antibodies (scale bar: 0.3 µm). (A′,A″) On the ODF2 ring, the arrow points toward the center of the centriolin signals and corresponds with BB orientation. (A″) Example showing the determination of BB orientation in an actual image (same image as B, bottom). (B) 12-week-old WT MCC stained with anti-ODF2 (magenta) and anti-centriolin (green) antibodies. Images were manually tiled because the cell could not be captured in one field, and maximum intensity projection (MIP) images (rendered using up to 15 slices acquired at a step size of 0.1 µm to cover all centriolin and ODF2 signals) are shown. The top row shows the original image (scale bar: 1 µm) while the bottom row shows the high magnification image (scale bar: 0.5 µm). In this cell, 210 BBs were analysed and the CV was 0.08. The ovarian and uterine sides are on the left and the right, respectively, in all figures (shown as O→U). (B′) *Celsr1*$^{-/-}$ mutant; 121 BBs were analysed (CV=0.25). (C,C′) Small arrows indicate BB orientation in cells shown in B and B′. The mean BB orientation is indicated by the large arrow, and the arrow color represents the CV value of the cell. (D) Variation in the orientation of BBs in each cell was evaluated as CV. CV values range from 0 (totally unidirectional) to 1 (no bias). Each point on the graph corresponds to one cell and the red horizontal bar represents the median. The colors are used to indicate the CV value of each cell when showing the mean BB orientation of the cell with the arrow, as shown in Fig. 1C,C′ and E,E′. Twenty cells from two animals were analysed for both genotypes. The datasets are identical to those shown in Fig. S5. (E,E′) Representatives of mean BB orientation in neighboring WT cells and *Celsr1*$^{-/-}$ cells, respectively. Tiled images were used to compare angles between cells. The mean BB orientation of each cell is shown with an arrow, and the arrow colors represent the CV values shown in the bottom right inset.

towards the region of microtubule enrichment near the apical surface, and CELSR1 plays a role in aligning the orientation of microtubule enrichment between cells.

Connection between microtubules and BBs in oviduct MCCs

Electron microscopic observation of MCCs has previously shown that microtubules are attached to the tip of the BF and run along the

Journal of Cell Science (2021) 134, jcs257006. doi:10.1242/jcs.257006

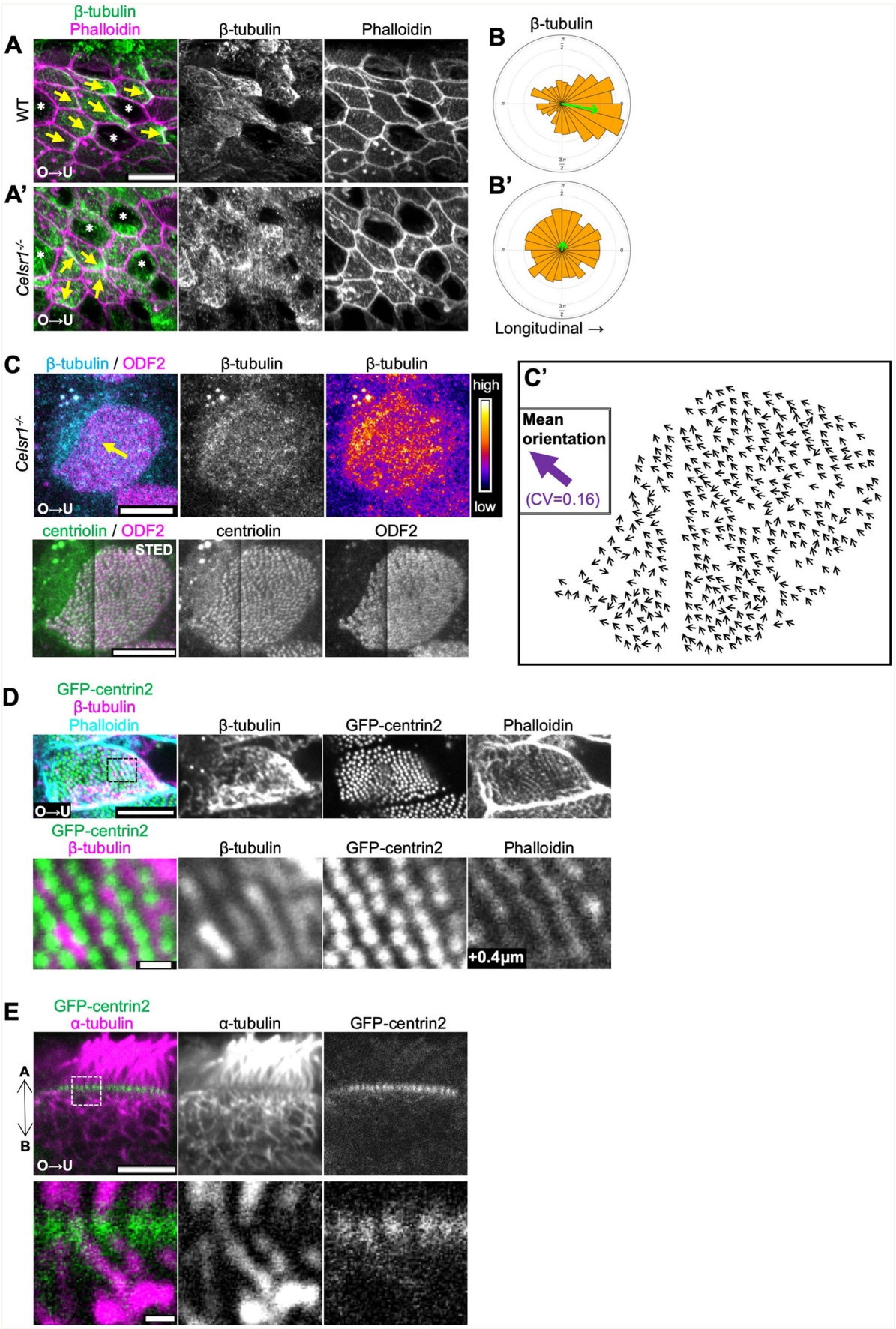

Fig. 2. See next page for legend.

Journal of Cell Science (2021) 134, jcs257006. doi:10.1242/jcs.257006

Fig. 2. Direction of polarized microtubule enrichment correlated with BB orientation in WT and *Celsr1*$^{-/-}$. (A,A′) Oviduct epithelium of adult (11-week-old) WT (A) and *Celsr1*$^{-/-}$ mutant (A′) stained with anti-β-tubulin (green) and phalloidin (magenta). MIP images were created from 20 images acquired at a step size of 0.2 µm (scale bar: 10 µm). The direction of β-tubulin enrichment is shown with yellow arrows. Secretory cells are indicated with white asterisks. (B,B′) Rose diagrams show the results of quantifying the orientation of microtubule enrichment near the cell–cell boundary. The angles between the elongated folds (longitudinal axis of the folds) were measured. The angle was classified into 24 bins. The area of each bin is proportional to the number of cells within each bin. A total of 369 cells from three WT animals and 347 cells from three *Celsr1*$^{-/-}$ animals were analysed. The angle and the length of each green arrow indicate the mean angle and 1 – CV, respectively. (C) Top row, confocal images of the *Celsr1*$^{-/-}$ mutant MCC stained with anti-β-tubulin (blue) and anti-ODF2 (magenta) antibodies. MIP images were rendered from 10 images acquired at a step size of 0.3 µm. The yellow arrow indicates the orientation of microtubule enrichment. Bottom row, super-resolution microscopy images stained with anti-ODF2 (magenta) and anti-centriolin (green) antibodies. MIP images were rendered from 20 images acquired at a step size of 0.1 µm. To obtain centriolin signals, the fixation condition was different from that used for Fig. 2A,A′ (scale bar: 5 µm). Images shown were manually tiled from two images. (C′) Small arrows indicate BB orientation, and color of the large arrow in the inset represents the mean BB orientation. (D,E) Apical view (D) and lateral view (E) of a MCC of a transgenic mouse expressing GFP-centrin2 (green) stained with anti-β-tubulin (magenta in D) or anti-α-tubulin (magenta in E) antibodies and phalloidin (cyan). (D) Top row, MIP image was rendered from three images acquired at a step size of 0.2 µm; bottom row shows a single plane at high magnification. Focal plane of phalloidin was 0.4 µm basal to GFP-centrin2 and β-tubulin, and indicated as '+0.4 µm' in D. (E) Single plane images; bottom row shows high magnification after background subtraction. The apical side is located towards the top of each image (scale bars: 5 µm and 0.5 µm in the top and bottom rows, respectively, in D and E.).

apical surface interconnecting adjacent BF (Reed et al., 1984; Sandoz et al., 1988; Vladar et al., 2012; Herawati et al., 2016; Tateishi et al., 2017). It remains unclear, however, how the microtubules are connected to the BBs and how they are involved in organizing BB orientation. In order to determine microtubule localization and elucidate the relationship between microtubules and BB and BF in detail, microtubules and BBs were visualized using an anti-β-tubulin antibody and GFP-centrin2, respectively. Microtubules formed a striped pattern on the plane parallel to the apical surface in the range of 0.6 µm, which was identical to GFP-centrin2 (Fig. 2D; Movie 1). The signal intensities of the stripes were also stronger on the uterine side of each cell (Fig. 2D) and weaker on the ovarian side. When examined from the lateral side of the cells, a thick microtubule bundle (visualized with anti-α-tubulin antibody) connected to each BB (visualized with GFP-centrin2) extended to the basal side of the cell in the cytoplasm (Fig. 2E), although which components of microtubules visualized by lateral sections correspond to the apical microtubule stripes remains unclear. We also examined *Celsr1*$^{-/-}$ oviducts and found that the apical microtubule stripes were maintained, while apico-basal bundles were clearly connected to BBs (Fig. S1B,C). To summarize, oviduct MCCs have microtubules running along BBs as well as those extending basally from BBs, and either one of them, or both, are enriched at a cell boundary; CELSR1 is not involved in the assembly of these microtubules, although it is important for their PCP orientation.

CAMSAP3, a microtubule minus-end binding protein, localizes asymmetrically to the base of cilia

Although γ-tubulin localizes in BBs and BF (Muresan et al., 1993; Hagiwara et al., 2000), it is unknown if γ-tubulin regulates ciliary orientation (Yuba-Kubo et al., 2005). The minus-ends of axonemal microtubules are oriented towards the BBs in MCCs. In intestinal non-ciliated epithelial cells, the minus-ends of non-centrosomal microtubules that run apico-basally are anchored to the apical surface by CAMSAP3 (Meng et al., 2008), a non-centrosomal microtubule minus-end binding protein (Toya et al., 2016). Based on the above, we sought to determine if CAMSAP3 plays a role in MCCs and if it is involved in organizing microtubules to regulate the orientation of BBs.

We compared CAMSAP3 distribution with that of other BB and BF components. CAMSAP3 was detected on the uterine side of BBs labeled with GFP-centrin2, and these two signals were observed as pairs (Fig. 3A). In the lateral view, CAMSAP3 partially overlapped GFP-centrin2 on the apical side (Fig. 3A′). γ-tubulin localized to the uterine and basal sides of the GFP-centrin2, and these two were also paired (Fig. 3B,B′). When CAMSAP3 and γ-tubulin were compared directly, both signals were detected as small dots in the apical view (Fig. 3C). In the lateral view, these two signals were separated, and the CAMSAP3 signal showed apical localization relative to the γ-tubulin signal (Fig. 3C′). CAMSAP3 and γ-tubulin seemed to be paired, but the positional relationship between them was not constant in the *x*–*y* plane. This may be due to the longer distances between the two signals along the apico-basal axis, and the BB and axoneme were not always vertical relative to the apical surface. Hence the angles between these were variable (Fig. S2B, bottom panels, dotted lines) when observed from the lateral side. CAMSAP3 was detected as a small dot on the same side as centriolin, which was located away from the center of BBs using super-resolution microscopy (Fig. 3D). CAMSAP3 also showed apical localization relative to centriolin, and we observed CAMSAP3 signals on the uterine side of ODF2 (Fig. S2C).

The relative positions of CAMSAP3 and other BB and BF markers in mature MCCs are summarized in Fig. 3E. We observed that CAMSAP3 was located in the same direction as the BF from the apical view, but was located apically when compared with other BF markers such as centriolin.

CAMSAP3 protein localizes to the BB prior to coordination of BB orientation

We went on to determine CAMSAP3 localization and the coordination of BB orientation during the maturation of MCCs. BB orientation has been reported to be coordinated in each cell at the final process when BBs spread over the entire apical surface during the maturation of MCCs in mouse trachea (Herawati et al., 2016). We began by observing the maturation process of MCCs of mouse oviducts (Fig. 4; Fig. S3). We classified epithelial cells into five types based on the number and distribution of γ-tubulin and GFP-centrin2, which are present in BBs. Similar progression patterns were observed when GFP-centrin2 and γ-tubulin were used to visualize BBs (Fig. S3B). Strong signals were observed for γ-tubulin (one or two large foci) and GFP-centrin2 (multiple large foci) around the apical surface in type I cells (Fig. 4A; Fig. S3B). Ring-shaped signals and condensed small dots were observed on the apical side of the nucleus in type II and type III cells, respectively. Unevenly scattered dots that formed clusters were observed around the apical surface of type IV cells, while dots were scattered across the apical surface in type V cells. The ratio of type V cells increased as development progressed. At postnatal day 13 (P13), all cell types were observed. These analyses along the developmental stages suggested the progression of cell types from type I through to type V. Time-lapse observation of *GFP-CETN2* mice also suggested cell type transition from type I to type V (Fig. S3C; Movie 2).

Next, we analysed when CAMSAP3 became co-localized with the BB components during the development of MCCs. In P13 oviducts, CAMSAP3 showed dot-like signals around the apical

Journal of Cell Science (2021) 134, jcs257006. doi:10.1242/jcs.257006

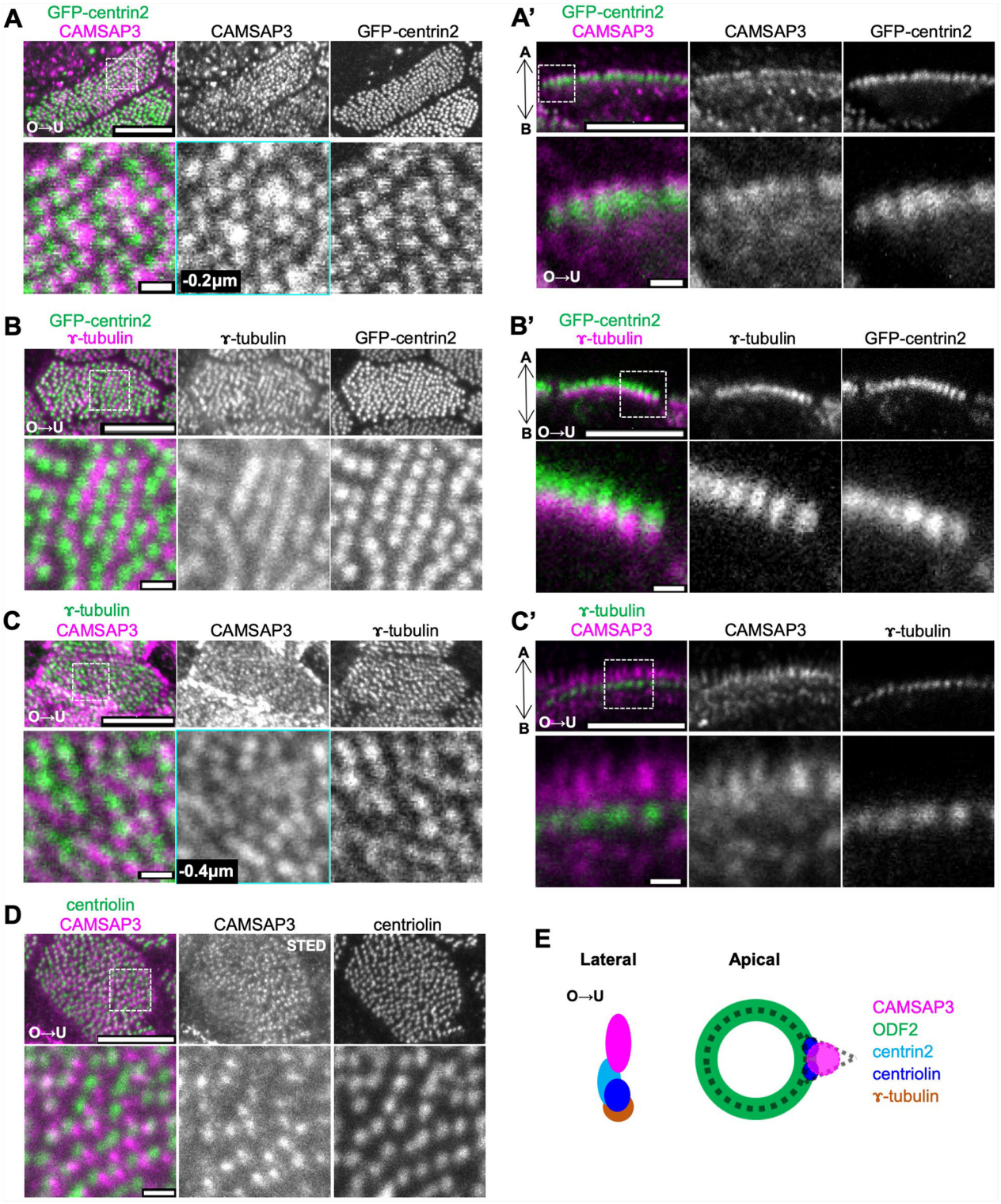

Fig. 3. See next page for legend.

surface in all cell types (Fig. 4B). This apical localization of CAMSAP3 in the oviduct MCCs was similar to that reported in adult nasal respiratory epithelia, but we did not observe CAMSAP3 localized in two layers during the early stage of development as reported (Robinson et al., 2020). In type IV and type V cells, CAMSAP3 was observed adjacent to GFP-centrin2. CAMSAP3 signal intensity was stronger in type IV than in type V cells, and CAMSAP3 dots were widely distributed over the apical surface while GFP-centrin2 formed clusters of dots. In type V cells, CAMSAP3 localized at BBs, which was similar to their observed localization in adult MCCs, while CAMSAP3 dots were even smaller when compared with those in adult MCCs. These results suggest that CAMSAP3 localizes to BBs both during and after BB docking to the cell surface.

Journal of Cell Science (2021) 134, jcs257006. doi:10.1242/jcs.257006

Fig. 3. Localization of CAMSAP3 and other BB proteins in oviduct MCCs. Images taken from the apical side (A–D) and lateral side (A′–C′) of MCCs are shown. (A,A′) Confocal images of the MCCs of adult transgenic mice expressing GFP-centrin2 (green) stained with anti-CAMSAP3 antibody (magenta). (A) Top, MIP image rendered from two images acquired at a step size of 0.2 µm; bottom, magnified single plane images of the boxed region in A,A′. The focal plane of CAMSAP3 was 0.2 µm apical to the plane of GFP-centrin2, and is indicated as '–0.2 µm' (cyan frame). (B,B′) Staining with anti-γ-tubulin antibody (magenta). (B) Top, MIP image rendered from eight images acquired at a step size of 0.2 µm; bottom, magnified images of the boxed region in B. (C,C′) WT adult MCCs stained with anti-CAMSAP3 (magenta) and anti-γ-tubulin (green) antibodies. (C) Top, MIP image rendered from six images acquired at a step size of 0.2 µm; bottom, focal plane of CAMSAP3 was 0.4 µm apical to the focal plane of γ-tubulin, and is indicated as '–0.4 µm' (cyan frame). (D) Anti-centriolin (green) and anti-CAMSAP3 (magenta) antibody staining. CAMSAP3 and centriolin signals were acquired by STED and confocal microscopy, respectively. MIP images were rendered from 13 images acquired at a step size of 0.2 µm (scale bars: 5 µm in upper panels and 0.5 µm in lower panels, respectively, of A–D and A′–C′). Also see Fig. S2. (E) Schematic diagram showing the localization of CAMSAP3 and other BB and BF proteins. The relative position of molecules is shown. This schematic was drawn based on the observation with confocal and super-resolution microscopy. The scale is different between lateral and apical views, and the apical view corresponds to ×3 magnified.

We also examined the localization of ODF2 and centriolin using P13 mouse oviducts (Fig. S3E,F). Centriolin colocalized with GFP-centrin2 in all cell types; however, ODF2 and centriolin colocalized only in type IV and type V cells (Fig. S3F). ODF2 localized to BBs in 83% of type IV cells, and 100% of type V cells. The above results indicate that CAMSAP3 localizes to the BB at a later time than other BB and BF components, including centrin2, centriolin and γ-tubulin, which were already colocalized before BB docking. ODF2, however, localizes to BBs later than CAMSAP3.

We next focused on type IV and type V cells and determined BB orientation (Fig. 4C–E). In type IV cells, individual BBs were oriented in various directions within each cell, and CV values varied widely between 0.2 and 0.9 (n=28 cells, median=0.53). In type V cells, however, BBs were oriented in a similar direction, and the CV value of most cells was smaller than 0.32 (n=28 cells, median=0.13) (Fig. 4E). Thus, BB orientation was aligned during the transition from type IV to type V. Taken together, these observations revealed that CAMSAP3 localizes to the BBs during their docking to the plasma membranes prior to the coordination of BB orientation.

BB orientation is not coordinated in *Camsap3*$^{dc/dc}$ mutants

To determine whether CAMSAP3 plays a role in coordination of BB orientation, we examined MCCs in the *Camsap3*$^{dc/dc}$ mutant (Toya et al., 2016) oviduct. In the *Camsap3dc* allele, the genomic region for exons 14 to 17, which encodes CKK domain, was deleted. We found that multi-cilia formed in *Camsap3*$^{dc/dc}$ on the luminal surface of the oviduct epithelium (average 221 BBs per cell, s.d.=33.3, n=20 cells, two animals). The distribution of BBs in each mutant MCC was not aligned compared with WT (Fig. 5A,A′). The BB orientation in each cell was not in the same direction in the mutants (Fig. 5B,B′), and CV values varied from 0.1 to 0.9. Compared with the CV in WT littermates (median=0.11, n=20 cells, average 200 BBs per cell analysed), the CV values were significantly higher in *Camsap3*$^{dc/dc}$ mutants (median=0.44, n=20 cells, average 182 BBs per cell analysed; Fig. 5C; Fig. S5). The CV value for *Camsap3*$^{dc/dc}$ mutants was also significantly higher than that of the *Celsr1*$^{-/-}$ mutant and was comparable to WT immature type IV cells (Fig. S5). BBs were distributed across the entire apical surface in *Camsap3*$^{dc/dc}$ mutants, which is different from WT immature type IV MCCs, whereas BBs formed clusters, suggesting that high CV is not due to the delay in MCC maturation. The mean BB orientation of each cell was aligned between cells along the longitudinal axis of the oviduct, even between cells with higher CV values (Fig. 5D,D′). The mean BB orientation was also aligned with the direction of the oviduct folds (data not shown).

Electron microscopy observations also revealed BB orientation defects in the *Camsap3*$^{dc/dc}$ mutant (Fig. 5E,E′), and were consistent with the results obtained using super-resolution microscopy. Similar results were recently reported in mouse nasal epithelium and in *Xenopus* after *Camsap3* gene inactivation (Robinson et al., 2020). In a minor population, we observed structures similar to the BF protruding from multiple positions on BBs (Fig. S4A). Pronounced defects in assembly of the central pair were reported in the nasal MCCs (Robinson et al., 2020), although such abnormalities were much less evident in the oviduct MCCs (Fig. S4B). These results indicate that CAMSAP3 is indispensable for aligning BB orientation in each cell.

Planar polarized protein localization is maintained in *Camsap3*$^{dc/dc}$

Next, we examined if PCP is maintained in *Camsap3*$^{dc/dc}$ mutant oviducts (Fig. 6A,A′). Cell shape was elongated and epithelial folds formed similarly to WT. PCP factors CELSR1 and VANGL1 localized to the cell boundary perpendicular to the ovary–uterine axis in a polarized fashion, in the same manner as in WT when they were quantified (Fig. 6B,B′). The enrichment of polarized microtubules near the cell boundary on the uterine side was also evident (Fig. 6C,D). Thus, despite the disruption of the coordinated BB orientation, PCP factors and microtubule enrichment occurred in a normal orientation in the mutant oviducts. These results suggest that the *Camsap3*$^{dc/dc}$ mutant phenotype is not due to the loss of PCP at the tissue level.

Apical microtubule distribution is disturbed in *Camsap3*$^{dc/dc}$ mutant MCCs

To elucidate the mechanism of how CAMSAP3 coordinates cilia orientation within cells, we examined the distribution of microtubules more closely in *Camsap3*$^{dc/dc}$ mutant MCCs, as it might be related to the disorganization of BB orientation. In *Camsap3*$^{dc/dc}$ mutants, α-tubulin was distributed to fill the spaces between GFP-centrin2 signals as observed in WT. Notably, however, microtubule stripes became fragmented in the mutant cells (Fig. 6E′), although some of BBs were still aligned in rows (Fig. 6E,E′, dashed lines). The analysis of the overall staining intensity of α-tubulin located at the level of GFP-centrin2 in individual cells (in the range of 0.6 µm) showed that, while α-tubulin was enriched at the uterine side of WT cells, this enrichment was no longer observed in *Camsap3*$^{dc/dc}$ cells (compare α-tubulin panels in Fig. 6F,F′), although other microtubule populations still exhibited a gradient distribution as shown in Fig. 6C. We next examined the microtubules, which extend apico-basally into the cytoplasm from BBs, from the lateral side (Fig. 6G,G′), finding that the assembly of this population of microtubules looked normal in *Camsap3*$^{dc/dc}$ mice. We also checked for acetylation of microtubules by staining with anti-acetylated tubulin antibody, but we did not detect any differences between WT and mutant mice (Fig. S4E, E′). These observations suggest that the assembly of microtubules horizontally associated with BBs are selectively regulated by CAMSAP3.

As a previous study showed that CAMSAP3 binds actin filaments via ACF7 (also known as MACF1; Ning et al., 2016), we observed actin distribution using phalloidin. Phalloidin signals also formed

Journal of Cell Science (2021) 134, jcs257006. doi:10.1242/jcs.257006

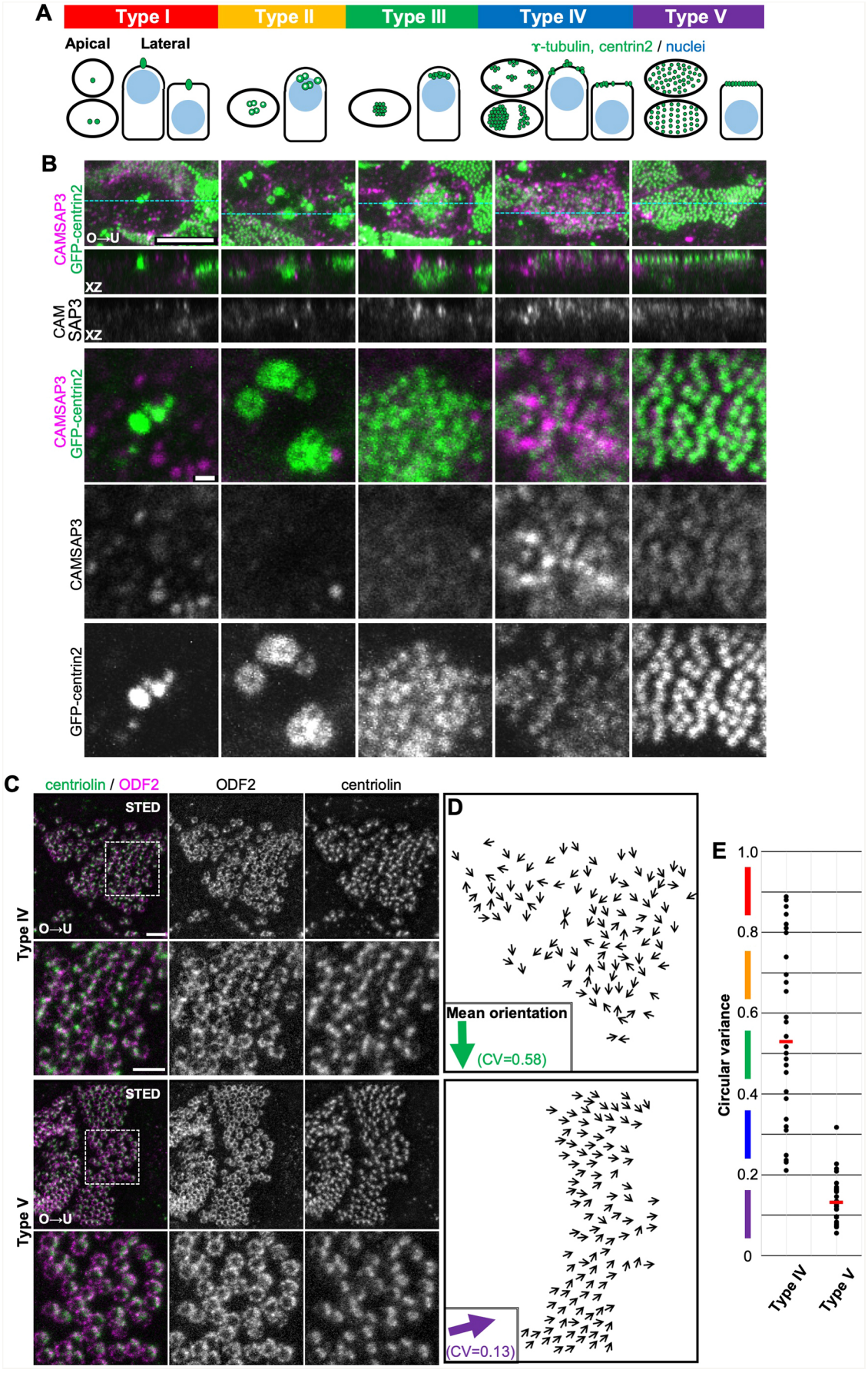

Fig. 4. See next page for legend.

Journal of Cell Science

Journal of Cell Science (2021) 134, jcs257006. doi:10.1242/jcs.257006

Fig. 4. CAMSAP3 protein localization during maturation of MCCs. (A) Schematic diagram of cell types observed on postnatal day 13 (P13). Cells were classified into five types based on cell shape, nuclear position and GFP-centrin2 or γ-tubulin distribution. (B) Confocal images of GFP-centrin2 (green) and anti-CAMSAP3 antibody staining (magenta). Images were acquired and processed under the same conditions to enable direct comparison of signal intensities. Top, MIP images rendered from 20 images acquired at a step size of 0.2 µm. Panels in the second and third rows show *x*–*z* images along the blue dashed lines in the top row. Bottom three panels show the single focal plane where the GFP-centrin2 signal was observed. See also Fig. S3. Scale bars: 0.5 µm. (C) Super-resolution microscopic images of P13 WT cells stained with anti-centriolin (green) and anti-ODF2 (magenta) antibodies. MIP images rendered from 15 images acquired at a step size of 0.1 µm after each image was subjected to displacement correction (Fiji menu command Correct 3D Drift) (scale bar: 1 µm). Magnified images of boxed regions in the top panels are shown in the bottom panels (scale bar: 0.5 µm). (D) Direction of BB orientation. Number of BBs analysed and CV in the representative images: *n*=108 and CV=0.58 (type IV); *n*=107 and CV=0.13 (type V). (E) Distribution of CVs in type IV and type V cells. Each dot in the graph corresponds to one cell, and the horizontal red bar represents the median. Three animals were analysed. Type IV: 28 cells (average number of BB analysed per cell=97; median CV=0.53 indicated with horizontal red bar). Type V: 28 cells (average number of BB analysed per cell=116; median CV=0.13). The datasets are identical to those in Fig. S5.

stripes about 0.2 µm basal from the plane of α-tubulin stripes in WT (Fig. 6E), whereas in *Camsap3*$^{dc/dc}$, the distributions of α-tubulin and phalloidin signals became less identical (Fig. 6E′, arrowheads). At the apical surface of MCCs, phalloidin-positive protrusions were observed more frequently in the mutant cells (Fig. S4C,C′). A small number of these protrusions showed a cyst-like structure, and the cysts occasionally contained microtubules or multiple axonemes (Fig. S4C′,D), which are never seen in WT cells. These suggest that actin filament organization was also affected as a result of *Camsap3* mutation. Finally, we observed the distribution of CAMSAP3 in *Celsr1*$^{-/-}$ MCCs, and found no change in its distribution after CELSR1 loss (Fig. S6A,A′), implying that the CELSR1 and CAMSAP3 systems differentially regulate BB orientation.

DISCUSSION

The present study analysed BB orientation and its coordination in the oviducts using two mutants which have lost CELSR1 or CAMSAP3 functions. Each mutant displayed distinct abnormalities concerning these processes. In *Celsr1* mutants, PCP was partly abrogated, whereas the intracellular polarity represented by BB orientation was moderately maintained within individual cells. *Camsap3*-mutated cells showed disruption of BB orientation in individual cells, but not losing PCP of the cell sheet. These observations suggest that BB orientation in individual cells occurs in the absence of CELSR1, and cooperation of the CELSR1 and CAMSAP3 systems is necessary to determine the entire polarity of oviducts at both cellular and tissue levels.

CELSR1 coordinates cilia orientation between cells in the oviduct

Fluid flow in the oviduct/fallopian tube was recently reported to be directed from the uterine side to the ovarian side by the secretion of fluid and contractility of smooth muscles in the isthmus of the oviduct (Hino and Yanagimachi, 2019). Eggs are transported steadily against the direction of fluid flow from the fimbria to the ampulla by directional movements of the cilia, which are coordinated both within individual cells and between cells. In this study, observing BBs with super-resolution microscopy (STED) allowed us to determine whether cilia orientation is coordinated between cells even in the wide field within the folds of the infundibulum epithelium. We confirmed that cilia orientation is aligned with organ orientation, i.e. the longitudinal axis of the oviduct in the infundibulum.

The mechanism for coordinating the orientation of multi-cilia differs between animal species and between organs. Boutin and colleagues have reported that the functions of PCP factors also vary within a tissue (Boutin et al., 2014). In the mammalian ependyma, one group of PCP factors [CELSR2, CELSR3, FZD3 (frizzled-3) and VANGL2] regulates cilia orientation within individual cells, while another group (CELSR1, FZD3 and VANGL2) regulates cilia orientation between cells.

The involvement of CELSR1 in the coordination of cilia orientation may differ between ependyma and oviduct epithelium. While cilia patch displacement and microtubule enrichment were correlated in *Celsr1*$^{-/-}$ ependyma, the orientation of patch displacement did not correlate with mean cilia orientation. In contrast, the direction of microtubule enrichment was not coordinated between oviduct cells in *Celsr1*$^{-/-}$, while the mean BB orientation coincided with the direction of microtubule enrichment. Among the CELSR family proteins, CELSR1 probably plays a major role in coordinating cilia orientation in the oviduct epithelium because CELSR3 expression was not detected, and *Celsr2* mutants have no obvious ciliary phenotype in the oviduct. Cilia orientation was moderately coordinated in individual cells lacking CELSR1, but the orientation between cells was not the same. This suggests that CELSR1 is mainly responsible for coordinating cilia orientation between cells.

We cannot rule out the possibility that other PCP factors may coordinate cilia orientation within each cell. However, even when *Vangl2* is deficient, oviduct MCCs do not show visible abnormalities (F.M.U., M.A. and T.F., unpublished data), in contrast to ependymal MCCs. We also have previously reported that in *Celsr1*$^{-/-}$ mutants, VANGL2 proteins weakly localized on the cell membrane, but the distribution was more uniform (Shi et al., 2014), suggesting that the function of VANGL2 is also partly affected. FZD6 was distributed unevenly in *Celsr1*$^{-/-}$ oviduct MCCs (data not shown), and this localized FZD6 may be regulating intracellular BB organization. Another possibility is that intracellular coordination of cilia orientation in oviduct MCCs is less dependent on PCP factors.

Microtubule networks and the regulation of cilia orientation in individual cells by CAMSAP3

Cells that lack CELSR1 were proposed to retain the ability to self-organize the distribution and orientation of cilia within individual cells. In mammalian MCCs found in the ependyma and trachea, microtubules are considered important for aligning cilia orientation within the cells (Clare et al., 2014; Herawati et al., 2016; Tateishi et al., 2017). These microtubules that localize just below the apical surface are connected to the BF. Microtubules are also enriched on one side of cells in a region that is slightly deeper than the apical microtubule meshwork around the cell–cell boundaries. We found that this is also common in oviduct MCCs. Moreover, we observed that microtubules are concentrated on the uterine side of each cell, and the apical microtubule meshwork forms a striped pattern with a gradient from the uterine side along the longitudinal axis of the oviduct. We found that in the *Celsr1*$^{-/-}$ mutant, microtubule stripes were present between the BBs (Fig. S6B), and microtubule enrichment was also conserved in more than 75% of MCCs. BBs were oriented towards the site of microtubule enrichment in these cells. These results suggest that CELSR1 is not essential for intracellular microtubule enrichment and apical stripe formation.

Journal of Cell Science (2021) 134, jcs257006. doi:10.1242/jcs.257006

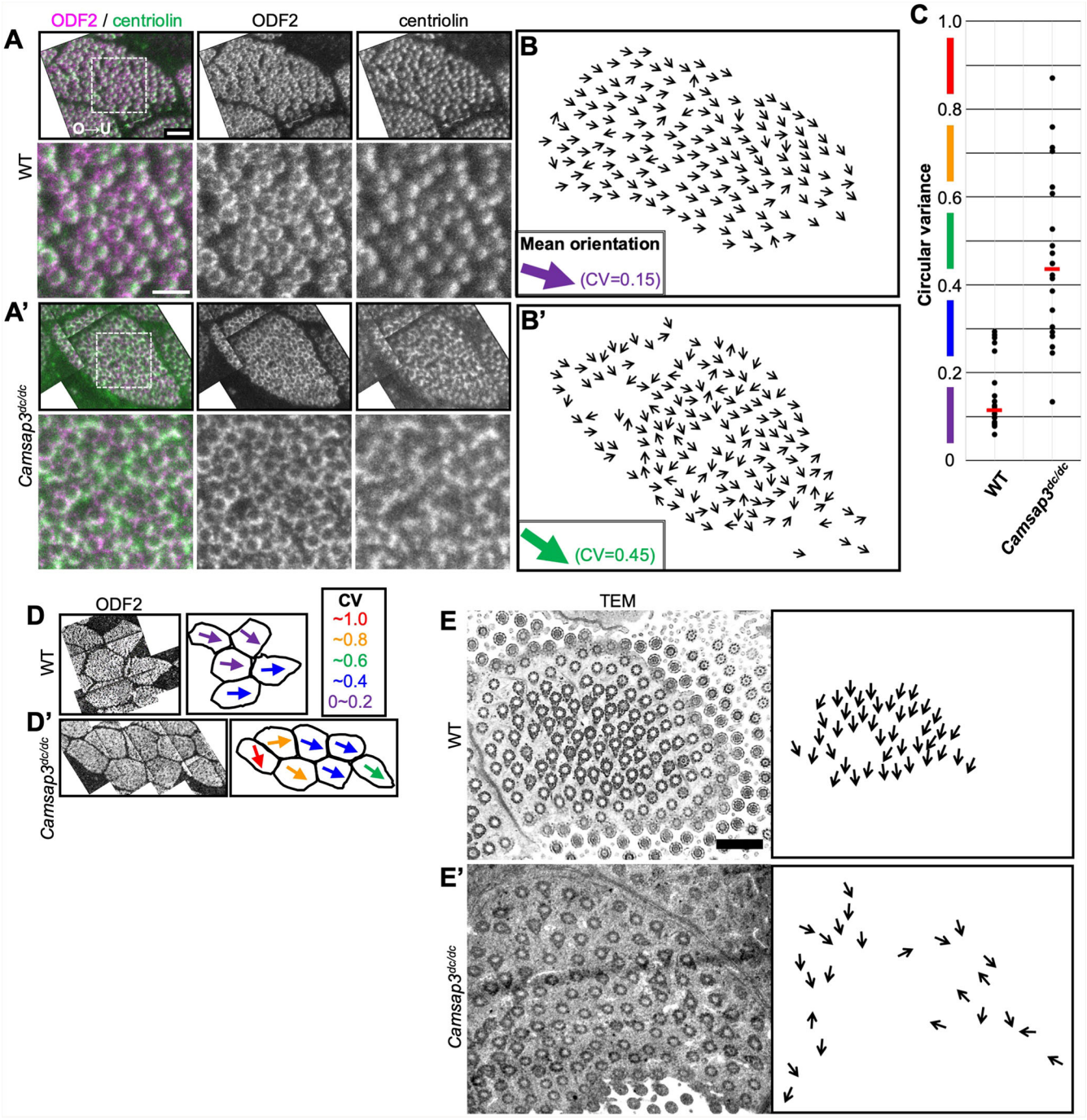

Fig. 5. BB orientation is not coordinated within each *Camsap3*$^{dc/dc}$ cell. (A,A′) Super-resolution microscopy (STED) images of adult WT (A) and *Camsap3*$^{dc/dc}$ mutant (A′) MCCs stained with anti-ODF2 (magenta) and anti-centriolin (green) antibodies. MIP images are rendered from 10–15 images acquired at a step size of 0.1 µm. Images shown were manually tiled from multiple images. Scale bars: 1 µm (upper panels) and 0.5 µm (lower panels). (B,B′) Orientation of BBs in A,A′. In these images, 148 BBs were analysed and CV=0.15 in WT, and 148 BBs and CV=0.45 in *Camsap3*$^{dc/dc}$. (C) CVs of BB orientation in WT and *Camsap3*$^{dc/dc}$ mutant. Each dot in the graph corresponds to one cell, and the red horizontal bar represents the median. Twenty WT cells (average number of analysed BBs per cell=200) and 20 *Camsap3*$^{dc/dc}$ cells (182 BBs per cell) were analysed. The datasets are identical to those in Fig. S5. (D,D′) Comparison of mean BB orientation in WT (D) and *Camsap3*$^{dc/dc}$ (D′). The direction of the mean BB orientation of each cell is shown with arrows, and color corresponds to the CV value of each cell. Images shown were manually tiled from multiple images. (E,E′) Transmission electron microscope (TEM) images of BB and BF in WT and *Camsap3*$^{dc/dc}$. In the right-hand panels, arrows indicate BB directions traced manually from the electron microscope images (scale bar: 1 µm). Magnified image of E′ is shown in Fig. S4A.

We found that CAMSAP3, a non-centrosomal microtubule minus-end binding protein, localizes to the base of the cilia of MCCs as recently reported (Robinson et al., 2020), in addition to γ-tubulin, a centrosomal microtubule minus-end binding protein (Clare et al., 2014). γ-tubulin has been shown to be localized in the BF, and we found that CAMSAP3 also exists asymmetrically in the same direction as γ-tubulin in each BB in the plane that is more apical to the position of γ-tubulin. The apical microtubule stripes and CAMSAP3 are on the same plane, and CAMSAP3 may interact with microtubules in this plane. During the maturation of MCCs,

Journal of Cell Science (2021) 134, jcs257006. doi:10.1242/jcs.257006

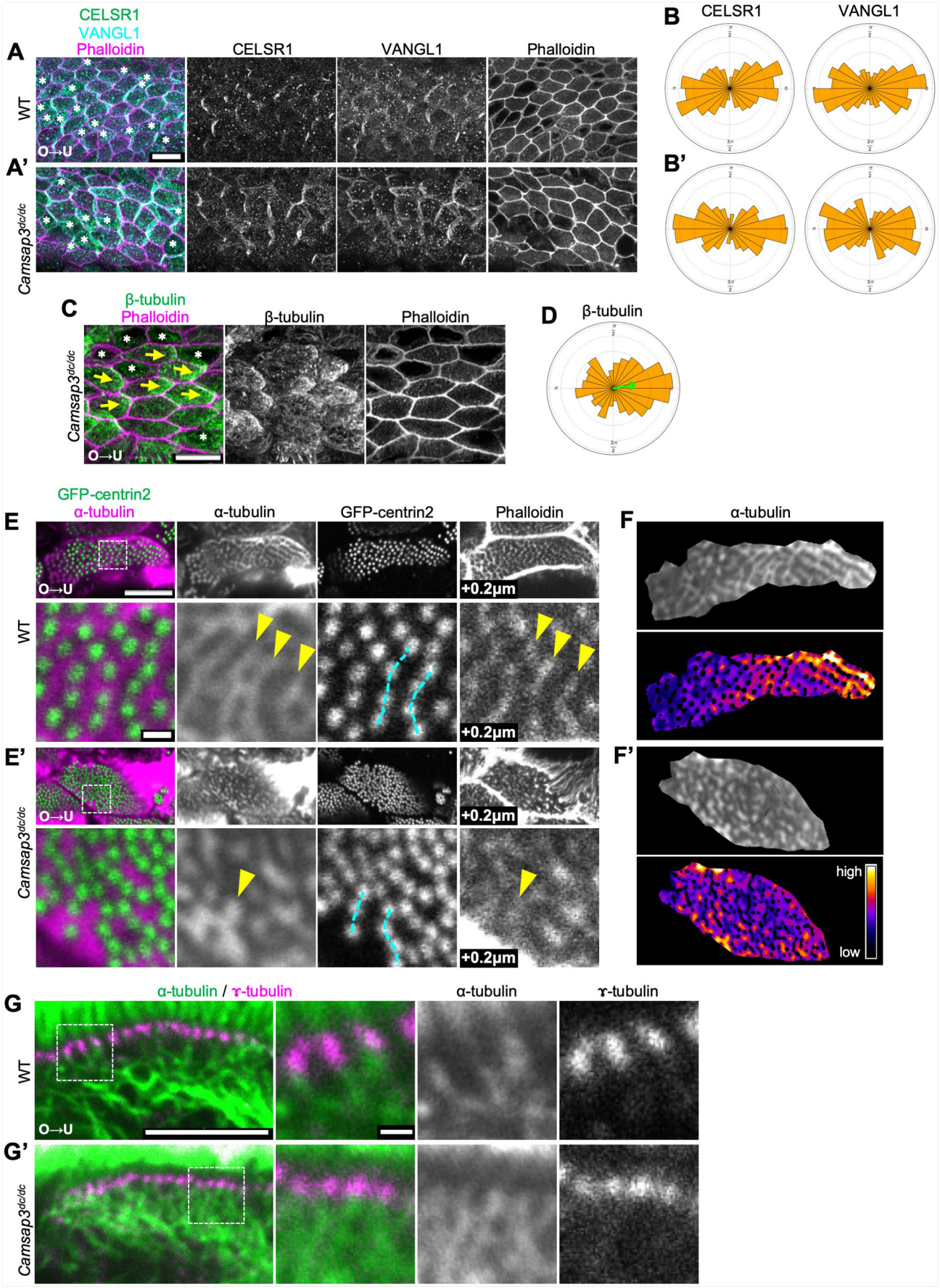

Fig. 6. See next page for legend.

Journal of Cell Science (2021) 134, jcs257006. doi:10.1242/jcs.257006

Fig. 6. Localization of proteins that regulate PCP is similar to wild-type, but the distribution of microtubules around BBs was altered in *Camsap3*$^{dc/dc}$ mutants. (A,A′) Confocal microscopy images of adult oviducts of littermate control (WT) and *Camsap3*$^{dc/dc}$ mutants stained with anti-CELSR1 (green), anti-VANGL1 (cyan) and phalloidin (magenta). MIP image is rendered from 15 images acquired at a step size of 0.2 µm (scale bar: 10 µm). Secretory cells are indicated with asterisks. (B,B′) Rose diagram showing the results of quantifying CELSR1 and VANGL1 localization. The angle was classified into 24 bins. The area of each bin is proportional to the number of cells distributed in each bin. A total of 99 WT cells and 119 *Camsap3*$^{dc/dc}$ cells were analysed. (C) Confocal images of adult *Camsap3*$^{dc/dc}$ oviduct stained with anti-β-tubulin antibody (green) and phalloidin (magenta). MIP images are rendered from 20 images acquired at a step size of 0.2 µm. The directions of β-tubulin enrichment are shown with yellow arrows. Secretory cells are indicated with white asterisks (scale bar: 10 µm). (D) Rose diagram showing the quantified direction of β-tubulin signal enrichment. (E,E′) Apical views of the oviducts from littermate WT (E) and *Camsap3*$^{dc/dc}$ (E′) mice showing GFP-centrin2 against background stained with anti-α-tubulin antibody and phalloidin. Magnified images of boxed regions in the upper panels are shown in the bottom panels. Images of two representative focal planes are shown. The focal plane of phalloidin signals was 0.2 µm basal (shown as '+0.2 µm') to the focal plane of α-tubulin and GFP-centrin2 signals. Note that striped microtubule signals are located to the side of aligned BBs (highlighted by cyan dashed lines) in WT but not in *Camsap3*$^{dc/dc}$. Distribution of microtubules and phalloidin signals are comparable in WT but not in *Camsap3*$^{dc/dc}$ (compare signals marked by yellow arrowheads). Scale bars: 5 µm (upper panels) and 0.5 µm (lower panels). (F,F′) Reconstructed images of α-tubulin signals located at the level of GFP-centrin2 signals. Different focal planes were merged for the reconstruction as the apical surface was not flat. Intensity of signals were color coded as shown in the bottom right inset. Position of GFP-centrin2 signals were masked to highlight the distribution of microtubules between BBs. (G,G′) Lateral views of WT (G) and *Camsap3*$^{dc/dc}$ (G′) MCCs stained with anti-α-tubulin (green) and anti-γ-tubulin (magenta) antibodies (scale bar: 5 µm). Magnified images of boxed region in the left-hand panels are shown in the right-hand panels (scale bar: 0.5 µm).

γ-tubulin exists in the BB regardless of the stage, but CAMSAP3 only localizes to BBs at the stage of BB docking onwards. Whereas the subcellular localization of γ-tubulin, centrin2 and centriolin were similar at all stages even when BBs were within the cytoplasm, CAMSAP3 was present on the apical region throughout all stages. From the above, it is suggested that γ-tubulin and CAMSAP3 may play different roles in organizing microtubules in MCCs. In intestinal epithelial cells that do not have multiple cilia, the absence of CAMSAP3 affected microtubules which run from the basal and attach to the apical surface (Toya and Takeichi, 2016), whereas the microtubules running apicobasally were maintained in *Camsap3*$^{dc/dc}$ mutant oviduct MCCs. However, the distribution of apical microtubules around BBs was disturbed. The intracellular orientation of cilia was not aligned in the oviduct, as reported in nasal respiratory epithelia (Robinson et al., 2020). This suggests a functional link between cilia orientation within individual cells and microtubule distribution in the apical surface. We speculate that the minus-end of microtubules running apicobasally may be bound to γ-tubulin in MCCs, but this needs to be elucidated in the future.

Why is cilia orientation disturbed in the *Camsap3* mutant?

Intracellular BB orientation was disorganized within individual cells in the *Camsap3* mutant. It is unlikely that the cells lacking CAMSAP3 disrupt planar polarity. Aside from cilia orientation, other patterning elements look undisturbed including localization of PCP factors, enrichment of microtubules on the cell edge and folds along the longitudinal axis of the oviduct.

Both CAMSAP3 and ODF2 may become localized to BBs when the polarity or asymmetry of BBs is established. In *Odf2* mutant tracheal MCCs, the BF structure is also lost, and ODF2 is essential for the polar formation of BBs (Kunimoto et al., 2012). CAMSAP3 is, however, dispensable for the BF formation, because the structure of BBs and the BF is almost normal except for some minor populations in *Camsap3*$^{dc/dc}$. BB/BF components (ODF2, centriolin, centrin2, γ-tubulin) localize to BBs in the absence of CAMSAP3. We observed some BBs with multiple BF only in *Camsap3* mutants; these BBs look similar to 'hybrid type BBs' reported recently (Liu et al., 2020), and may be increased in the *Camsap3*-deficient conditions. Otherwise, CAMSAP3 may also be responsible for limiting BBs to a single BF.

The BB orientation defect is probably due to local abnormalities around BBs. To align BBs and coordinate orientation of BBs, BF should be connected in the same orientation by cytoskeletal elements. One possibility is that CAMSAP3 is involved in anchoring BF to microtubule networks. We observed the impaired accumulation of microtubules in the apical region around BBs in *Camsap3*$^{dc/dc}$ mutant MCCs. We speculate that stable apical microtubule stripe formation is disrupted or the stability of apical microtubules are defective in the absence of CAMSAP3. Due to this change, the BF cannot anchor stably to the cytoskeleton, and the orientation of BBs are not aligned. The binding of CAMSAP3 and ACF7 may mediate the interaction between microtubules and actin filaments (Ning et al., 2016; Noordstra et al., 2016) and this interaction may also help microtubules to accumulate around BBs and connect neighboring BF in the same orientation. The stable accumulation of apical microtubules connecting the BF may therefore be the major function of CAMSAP3.

The mechanism for aligning cilia orientation within and between cells

In this study, we propose that the orientation of multi-cilia is regulated intracellularly and intercellularly. The direction of cilia has been suggested to be autonomously aligned within individual cells, regulated by CAMSAP3. CELSR1 is a PCP factor that aligns microtubule networks between cells to coordinate tissue-wide cilia orientation. Thus, both CELSR1 and CAMSAP3 systems are necessary to organize cilia orientation within a tissue. CAMSAP3 may be responsible for integrating polarity signals locally around the BBs downstream from PCP signals including CELSR1 via microtubules, as discussed in a previous report (Kunimoto et al., 2012). We tried to analyse interaction between these two mechanisms by making double knockouts, but we could not obtain the *Camsap3*$^{dc/dc}$–*Celsr1*$^{-/-}$ mice because they were perinatal lethal. In addition to these two hierarchies, microtubules are enriched at cell boundaries in a polarized fashion and form a concentration gradient inside cells, and these may connect the two systems. How these multi-scale mechanisms are connected so that the orientation of cilia in the whole tissue is aligned should be elucidated in the future.

MATERIALS AND METHODS

Animals

Female mice (Slc:ICR; SLC, Japan) were used to study MCCs in WT. *Celsr1*$^{-/-}$ mutant mice (Ravni et al., 2009), *Camsap3*$^{dc/dc}$ mutant mice (Toya et al., 2016) and *GFP-Centrin2* (*GFP-CETN2*) Tg mice (a gift from Holden Higginbotham, Brigham Young University - Idaho, Rexburg, ID, USA; transferred from Hiroshi Hamada, RIKEN Center for Biosystems Dynamics Research, Japan; Higginbotham et al., 2004) were described previously. Animal care and experiments were conducted in accordance with the Guidelines of Animal Experimentation of National Institutes for Natural Sciences and RIKEN animal experimentation guidelines. All animal experiments were approved by either the Animal Research Committee of National Institutes for Natural Sciences or by the Institutional Animal Care

and Use Committee of Riken Kobe Branch, respectively. Animals were maintained in a light- and temperature-controlled room using a 12 h:12 h light:dark cycle at 23±2°C.

Immunohistochemistry

The fluorescent images were taken using a Nikon A1 confocal microscope and TCS SP8 STED (Leica). Sample preparations were basically the same as previously reported (Shi et al., 2014). Anti-ODF2 antibody-producing hybridoma was a gift from Sachiko Tsukita, Osaka University, Japan (Tateishi et al., 2013). All primary antibodies and secondary antibodies used in this study are listed with fixation conditions in Table S1.

After 4% PFA fixation, samples were treated with 0.1% Triton X-100 in PBS at room temperature (RT) for 1 h. Fixed samples were blocked with Blocking One (Nacalai Tesque, Kyoto, Japan) at RT for 1 h, and incubated with primary antibodies in Blocking One at 4°C overnight. Incubation with α- or β-tubulin antibodies was for 36 h at 4°C. After washes with PBS, samples were incubated with secondary antibodies at RT for 3 h or 4°C overnight, or 24 h at 4°C for α- or β-tubulin antibody staining. After washes, each sample was mounted in Fluoromount-G (SouthernBiotech, Birmingham, AL, USA). ProLong Diamond (Thermo Fisher Scientific) was used to mount samples for STED observation. Detailed conditions for STED observation are shown in Table S1. The ovarian side of the oviduct was determined by the presence of fimbriae.

Quantifying the localization of PCP proteins and microtubule enrichment

Localization of PCP proteins was quantified by calculating nematic order as described (Aigouy et al., 2010; Shi et al., 2014). Maximum intensity projection (MIP) images were rendered from five serial images acquired with a step size of 1 µm. The orientation of microtubule enrichment was determined by using this method with minor modifications. As microtubules were enriched at the proximity of cell boundaries, cell boundaries were labeled with phalloidin and microtubule signals within the range of 0–5 pixels away from the cell boundaries were extracted using ImageJ. Nematic order defines only the axis and the magnitude of polarity. Additionally, the vector of microtubule polarity was determined by separating microtubule signals into two halves with a line perpendicular to the axis of the polarity, and by comparing intensities between these two separated microtubule signals. MIP images were rendered from 20 serial images acquired with a step size of 0.2 µm.

Quantifying basal body orientation

BB orientation was determined by ODF2 and centriolin signals after acquiring images with TCS SP8 STED (Leica). The detailed conditions for STED imaging are provided in Table S2. All images were acquired at a step size of 0.1 µm, and images from the ODF2 channel were subjected to an ImageJ macro (Correct 3D Drift). The same parameter of 'Correct 3D drift' was applied for images of centriolin. On each ODF2 ring, an arrow pointing to the center of ellipse/two points of centriolin signals (as shown in Fig. 1A′) was manually plotted. Making use of shape anisotropy of the arrow, the angle between the arrow and the longitudinal axis (ovary>uterus) of the oviduct was measured by Shape Descriptor Map (BioVoxxel_Toolbox; Fiji). In each cell, the CV of each set of angles was calculated using R as described previously (Zar, 2010; Shi et al., 2014). To acquire images using a transmission electron microscope (JEM-1010, Jeol; equipped with 2k×2k CCD camera, Olympus Soft Imaging Solutions), sample blocks were prepared as described (Shi et al., 2014). Ultrathin sections (50–70 nm) were made with a microtome (Leica EM UC7), and images were obtained on a grid (OkenShoji150-D, 75-A mesh). To measure the orientation of BB in transmission electron microscope images, an arrow was drawn manually from the center of BB to BF. CV was calculated as described above.

Time-lapse recordings of MCC maturation

The oviducts of *GFP-CETN2* Tg mice (postnatal day 13) were opened longitudinally, and placed in a drop of Dulbecco's modified Eagle's medium with high glucose (Gibco#31053) containing 10% FBS on a glass bottom dish (MatTek P35G-1.5-10-C). The drop was covered with liquid paraffin (128-04375, Wako) to avoid evaporation. The apical surface of the luminal epithelium faced the bottom of the dish. Oviducts were cultured at 37°C in 5% CO_2 during the recording, and imaged with a spinning disc confocal system (Cell Voyager CV1000; Yokogawa) using a 100× objective lens (UPLSPAPO100XS, Olympus) at 1 h intervals. At each time point, 40 slices were acquired at a step size of 0.5 µm.

Acknowledgements

We thank Holden Higginbotham and Hiroshi Hamada for the *GFP-Centrin2* mouse; Sachiko Tsukita for the anti-ODF2 antibody and hybridoma; Masahiko Itoh and Mikio Furuse for the anti-ZO1 antibody; Yoshikatsu Sato and Tetsuya Higashiyama (ABiS) for technical support and advice concerning STED microscopy; Gen Yamada for transmission electron microscope support; and Hiroko Saito, Azusa Kato, Tetsuhisa Otani and other laboratory members for technical support with animal care and helpful discussions. We also thank ExCELLS, the Spectrography and Bioimaging Facility (NIBB) and the EM facility (NIPS) for allowing us to use STED, confocal microscopes and an electron microscope, respectively.

Competing interests

The authors declare no competing or financial interests.

Author contributions

Conceptualization: F.M.U., M.A., T.F.; Methodology: F.M.U., M.A., D.S., T.F.; Software: M.A., D.S.; Investigation: F.M.U., D.S., Y.H.; Resources: S.O., Y.H., F.T., M.T.; Writing - original draft: F.M.U., M.A., M.T., T.F.; Writing - review & editing: F.M.U., M.A., T.F.; Visualization: F.M.U., M.A.; Supervision: M.T., T.F.; Project administration: T.F.; Funding acquisition: M.A., T.F.

Funding

This work was supported by the Japan Society for the Promotion of Science, KAKENHI (grant numbers 25291054, 15H01220, 17H03689, 16H06280 and 19K16153) and the Japan Science and Technology Agency, Core Research for Evolutional Science and Technology (JPMJCR1654 to T.F.).

Supplementary information

Supplementary information available online at
https://jcs.biologists.org/lookup/doi/10.1242/jcs.257006.supplemental

References

Aigouy, B., Farhadifar, R., Staple, D. B., Sagner, A., Röper, J.-C., Julicher, F. and Eaton, S. (2010). Cell flow reorients the axis of planar polarity in the wing epithelium of *Drosophila*. *Cell* **142**, 773-786. doi:10.1016/j.cell.2010.07.042

Antoniades, I., Stylianou, P. and Skourides, P. A. (2014). Making the connection: ciliary adhesion complexes anchor basal bodies to the actin cytoskeleton. *Dev. Cell* **28**, 70-80. doi:10.1016/j.devcel.2013.12.003

Aw, W. Y. and Devenport, D. (2017). Planar cell polarity: global inputs establishing cellular asymmetry. *Curr. Opin. Cell Biol.* **44**, 110-116. doi:10.1016/j.ceb.2016.08.002

Bayless, B. A., Navarro, F. M. and Winey, M. (2019). Motile cilia: innovation and insight from ciliate model organisms. *Front. Cell Dev. Biol.* **7**, 265. doi:10.3389/fcell.2019.00265

Boutin, C. and Kodjabachian, L. (2019). Biology of multi-ciliated cells. *Curr. Opin. Genet. Dev.* **56**, 1-7. doi:10.1016/j.gde.2019.04.006

Boutin, C., Goffinet, A. M. and Tissir, F. (2012). Celsr1-3 cadherins in PCP and brain development. *Curr. Top. Dev. Biol.* **101**, 161-183. doi:10.1016/B978-0-12-394592-1.00010-7

Boutin, C., Labedan, P., Dimidschstein, J., Richard, F., Cremer, H., Andre, P., Yang, Y., Montcouquiol, M., Goffinet, A. M. and Tissir, F. (2014). A dual role for planar cell polarity genes in ciliated cells. *Proc. Natl. Acad. Sci. USA* **111**, E3129-E3138. doi:10.1073/pnas.1404988111

Brooks, E. R. and Wallingford, J. B. (2014). Multi-ciliated cells. *Curr. Biol.* **24**, R973-R982. doi:10.1016/j.cub.2014.08.047

Butler, M. T. and Wallingford, J. B. (2017). Planar cell polarity in development and disease. *Nat. Rev. Mol. Cell Biol.* **18**, 375-388. doi:10.1038/nrm.2017.11

Chevalier, B., Adamiok, A., Mercey, O., Revinski, D. R., Zaragosi, L.-E., Pasini, A., Kodjabachian, L., Barbry, P. and Marcet, B. (2015). miR-34/449 control apical actin network formation during multi-ciliogenesis through small GTPase pathways. *Nat. Commun.* **6**, 8386. doi:10.1038/ncomms9386

Choksi, S. P., Lauter, G., Swoboda, P. and Roy, S. (2014). Switching on cilia: transcriptional networks regulating ciliogenesis. *Development* **141**, 1427-1441. doi:10.1242/dev.074666

Clare, D. K., Magescas, J., Piolot, T., Dumoux, M., Vesque, C., Pichard, E., Dang, T., Duvauchelle, B., Poirier, F. and Delacour, D. (2014). Basal foot MTOC organizes pillar MTs required for coordination of beating cilia. *Nat. Commun.* **5**, 4888. doi:10.1038/ncomms5888

Devenport, D. (2014). The cell biology of planar cell polarity. *J. Cell Biol.* **207**, 171-179. doi:10.1083/jcb.201408039

Garcia, G., III and Reiter, J. F. (2016). A primer on the mouse basal body. *Cilia* **5**, 17. doi:10.1186/s13630-016-0038-0

Guirao, B., Meunier, A., Mortaud, S., Aguilar, A., Corsi, J.-M., Strehl, L., Hirota, Y., Desoeuvre, A., Boutin, C., Han, Y.-G. et al. (2010). Coupling between hydrodynamic forces and planar cell polarity orients mammalian motile cilia. *Nat. Cell Biol.* **12**, 341-350. doi:10.1038/ncb2040

Hagiwara, H., Kano, A., Aoki, T., Ohwada, N. and Takata, K. (2000). Localization of gamma-tubulin to the basal foot associated with the basal body extending a cilium. *Histochem. J.* **32**, 669-671. doi:10.1023/A:1004163315822

Hale, R. and Strutt, D. (2015). Conservation of planar polarity pathway function across the animal kingdom. *Annu. Rev. Genet.* **49**, 529-551. doi:10.1146/annurev-genet-112414-055224

Henderson, D. J., Long, D. A. and Dean, C. H. (2018). Planar cell polarity in organ formation. *Curr. Opin. Cell Biol.* **55**, 96-103. doi:10.1016/j.ceb.2018.06.011

Herawati, E., Taniguchi, D., Kanoh, H., Tateishi, K., Ishihara, S. and Tsukita, S. (2016). Multi-ciliated cell basal bodies align in stereotypical patterns coordinated by the apical cytoskeleton. *J. Cell Biol.* **214**, 571-586. doi:10.1083/jcb.201601023

Higginbotham, H., Bielas, S., Tanaka, T. and Gleeson, J. G. (2004). Transgenic mouse line with green-fluorescent protein-labeled Centrin 2 allows visualization of the centrosome in living cells. *Transgenic Res.* **13**, 155-164. doi:10.1023/B:TRAG.0000026071.41735.8e

Hino, T. and Yanagimachi, R. (2019). Active peristaltic movements and fluid production of the mouse oviduct: their roles in fluid and sperm transport and fertilization. *Biol. Reprod.* **101**, 40-49. doi:10.1093/biolre/ioz061

Hirota, Y., Meunier, A., Huang, S., Shimozawa, T., Yamada, O., Kida, Y. S., Inoue, M., Ito, T., Kato, H., Sakaguchi, M. et al. (2010). Planar polarity of multi-ciliated ependymal cells involves the anterior migration of basal bodies regulated by non-muscle myosin II. *Development* **137**, 3037-3046. doi:10.1242/dev.050120

Iftode, F. and Fleury-Aubusson, A. (2003). Structural inheritance in *Paramecium*: ultrastructural evidence for basal body and associated rootlets polarity transmission through binary fission. *Biol. Cell* **95**, 39-51. doi:10.1016/S0248-4900(03)00005-4

Koyama, H., Shi, D. and Fujimori, T. (2019). Biophysics in oviduct: planar cell polarity, cilia, epithelial fold and tube morphogenesis, egg dynamics. *Biophys. Physicobiol.* **16**, 89-107. doi:10.2142/biophysico.16.0_89

Koyama, H., Shi, D., Suzuki, M., Ueno, N., Uemura, T. and Fujimori, T. (2016). Mechanical regulation of three-dimensional epithelial fold pattern formation in the mouse oviduct. *Biophys. J.* **111**, 650-665. doi:10.1016/j.bpj.2016.06.032

Kunimoto, K., Yamazaki, Y., Nishida, T., Shinohara, K., Ishikawa, H., Hasegawa, T., Okanoue, T., Hamada, H., Noda, T., Tamura, A. et al. (2012). Coordinated ciliary beating requires Odf2-mediated polarization of basal bodies via basal feet. *Cell* **148**, 189-200. doi:10.1016/j.cell.2011.10.052

Lemullois, M. and Marty, M. C. (1990). Immunocytochemical study of the formation of striated rootlets during ciliogenesis in quail oviduct. *J. Cell Sci.* **95**, 423-432.

Li, S. and Winuthayanon, W. (2016). Oviduct: roles in fertilization and early embryo development. *J. Endocrinol.* **232**, R1-R26. doi:10.1530/JOE-16-0302

Liu, Z., Nguyen, Q. P. H., Nanjundappa, R., Delgehyr, N., Megherbi, A., Doherty, R., Thompson, J., Jackson, C., Albulescu, A., Heng, Y. M. et al. (2020). Super-resolution microscopy and FIB-SEM imaging reveal parental centriole-derived, hybrid cilium in mammalian multi-ciliated cells. *Dev. Cell* **55**, 1-13. doi:10.1016/j.devcel.2020.09.023

Mazo, G., Soplop, N., Wang, W. J., Uryu, K. and Tsou, M. B. (2016). Spatial control of primary ciliogenesis by subdistal appendages alters sensation-associated properties of cilia. *Dev. Cell* **39**, 424-437. doi:10.1016/j.devcel.2016.10.006

Meng, W., Mushika, Y., Ichii, T. and Takeichi, M. (2008). Anchorage of microtubule minus ends to adherens junctions regulates epithelial cell-cell contacts. *Cell* **135**, 948-959. doi:10.1016/j.cell.2008.09.040

Meunier, A. and Azimzadeh, J. (2016). Multi-ciliated cells in animals. *Cold Spring Harb. Perspect Biol.* **8**, a028233. doi:10.1101/cshperspect.a028233

Mirzadeh, Z., Han, Y.-G., Soriano-Navarro, M., Garcia-Verdugo, J. M. and Alvarez-Buylla, A. (2010). Cilia organize ependymal planar polarity. *J. Neurosci.* **30**, 2600-2610. doi:10.1523/JNEUROSCI.3744-09.2010

Mitchell, B., Stubbs, J. L., Huisman, F., Taborek, P., Yu, C. and Kintner, C. (2009). The PCP pathway instructs the planar orientation of ciliated cells in the *Xenopus* larval skin. *Curr. Biol.* **19**, 924-929. doi:10.1016/j.cub.2009.04.018

Muresan, V., Joshi, H. C. and Besharse, J. C. (1993). Gamma-tubulin in differentiated cell types: localization in the vicinity of basal bodies in retinal photoreceptors and ciliated epithelia. *J. Cell Sci.* **104**, 1229-1237.

Ning, W., Yu, Y., Xu, H., Liu, X., Wang, D., Wang, J., Wang, Y. and Meng, W. (2016). The CAMSAP3-ACF7 complex couples noncentrosomal microtubules with actin filaments to coordinate their dynamics. *Dev. Cell* **39**, 61-74. doi:10.1016/j.devcel.2016.09.003

Noordstra, I., Liu, Q., Nijenhuis, W., Hua, S., Jiang, K., Baars, M., Remmelzwaal, S., Martin, M., Kapitein, L. C. and Akhmanova, A. (2016). Control of apico-basal epithelial polarity by the microtubule minus-end-binding protein CAMSAP3 and spectraplakin ACF7. *J. Cell Sci.* **129**, 4278-4288. doi:10.1242/jcs.194878

Ohata, S., Nakatani, J., Herranz-Pérez, V., Cheng, J., Belinson, H., Inubushi, T., Snider, W. D., García-Verdugo, J. M., Wynshaw-Boris, A. and Álvarez-Buylla, A. (2014). Loss of Dishevelleds disrupts planar polarity in ependymal motile cilia and results in hydrocephalus. *Neuron* **83**, 558-571. doi:10.1016/j.neuron.2014.06.022

Park, T. J., Mitchell, B. J., Abitua, P. B., Kintner, C. and Wallingford, J. B. (2008). Dishevelled controls apical docking and planar polarization of basal bodies in ciliated epithelial cells. *Nat. Genet.* **40**, 871-879. doi:10.1038/ng.104

Ravni, A., Qu, Y., Goffinet, A. M. and Tissir, F. (2009). Planar cell polarity cadherin Celsr1 regulates skin hair patterning in the mouse. *J. Invest. Dermatol.* **129**, 2507-2509. doi:10.1038/jid.2009.84

Reed, W., Avolio, J. and Satir, P. (1984). The cytoskeleton of the apical border of the lateral cells of freshwater mussel gill: structural integration of microtubule and actin filament-based organelles. *J. Cell Sci.* **68**, 1-33.

Reiter, J. F. and Leroux, M. R. (2017). Genes and molecular pathways underpinning ciliopathies. *Nat. Rev. Mol. Cell Biol.* **18**, 533-547. doi:10.1038/nrm.2017.60

Reiter, J. F., Blacque, O. E. and Leroux, M. R. (2012). The base of the cilium: roles for transition fibres and the transition zone in ciliary formation, maintenance and compartmentalization. *EMBO Rep.* **13**, 608-618. doi:10.1038/embor.2012.73

Robinson, A. M., Takahashi, S., Brotslaw, E. J., Ahmad, A., Ferrer, E., Procissi, D., Richter, C. P., Cheatham, M. A., Mitchell, B. J. and Zheng, J. (2020). CAMSAP3 facilitates basal body polarity and the formation of the central pair of microtubules in motile cilia. *Proc. Natl. Acad. Sci. USA* **117**, 13571-13579. doi:10.1073/pnas.1907335117

Sandoz, D., Chailley, B., Boisvieux-Ulrich, E., Lemullois, M., Laine, M.-C. and Bautista-Harris, G. (1988). Organization and functions of cytoskeleton in metazoan ciliated cells. *Biol. Cell* **63**, 183-193. doi:10.1016/0248-4900(88)90057-3

Shi, D., Arata, M. U., Fujimori, T. and Uemura, T. (2016a). Seven-pass transmembrane cadherin CELSRs, Fat4 and Dchs1 cadherins: from planar cell polatiry to three-dimensional organ architecture. In *The Cadherin Superfamily* (ed. S. Suzuki and S. Hirano), pp. 251-275. Springer.

Shi, D., Fujimori, T. and Uemura, T. (2013). Atypical cadherin negotiates a turn. *Dev. Cell* **26**, 1-2. doi:10.1016/j.devcel.2013.06.024

Shi, D., Komatsu, K., Hirao, M., Toyooka, Y., Koyama, H., Tissir, F., Goffinet, A. M., Uemura, T. and Fujimori, T. (2014). Celsr1 is required for the generation of polarity at multiple levels of the mouse oviduct. *Development* **141**, 4558-4568. doi:10.1242/dev.115659

Shi, D., Komatsu, K., Uemura, T. and Fujimori, T. (2011). Analysis of ciliary beat frequency and ovum transport ability in the mouse oviduct. *Genes Cells* **16**, 282-290. doi:10.1111/j.1365-2443.2011.01484.x

Shi, D., Usami, F., Komatsu, K., Oka, S., Abe, T., Uemura, T. and Fujimori, T. (2016b). Dynamics of planar cell polarity protein Vangl2 in the mouse oviduct epithelium. *Mech. Dev.* **141**, 78-89. doi:10.1016/j.mod.2016.05.002

Soh, A. W. J., van Dam, T. J. P., Stemm-Wolf, A. J., Pham, A. T., Morgan, G. P., O'Toole, E. T. and Pearson, C. G. (2019). Ciliary force-responsive striated fibers promote basal body connections and cortical interactions. *J. Cell Biol.* **219**, e201904091. doi:10.1083/jcb.201904091

Spassky, N. and Meunier, A. (2017). The development and functions of multi-ciliated epithelia. *Nat. Rev. Mol. Cell Biol.* **18**, 423-436. doi:10.1038/nrm.2017.21

Takagishi, M., Esaki, N., Takahashi, K. and Takahashi, M. (2020). Cytoplasmic dynein functions in planar polarization of basal bodies within ciliated cells. *iScience* **23**, 101213. doi:10.1016/j.isci.2020.101213

Takagishi, M., Sawada, M., Ohata, S., Asai, N., Enomoto, A., Takahashi, K., Weng, L., Ushida, K., Ara, H., Matsui, S. et al. (2017). Daple coordinates planar polarized microtubule dynamics in ependymal cells and contributes to hydrocephalus. *Cell Rep* **20**, 960-972. doi:10.1016/j.celrep.2017.06.089

Tateishi, K., Nishida, T., Inoue, K. and Tsukita, S. (2017). Three-dimensional organization of layered apical cytoskeletal networks associated with mouse airway tissue development. *Sci. Rep.* **7**, 43783. doi:10.1038/srep43783

Tateishi, K., Yamazaki, Y., Nishida, T., Watanabe, S., Kunimoto, K., Ishikawa, H. and Tsukita, S. (2013). Two appendages homologous between basal bodies and centrioles are formed using distinct Odf2 domains. *J. Cell Biol.* **203**, 417-425. doi:10.1083/jcb.201303071

Tissir, F., Qu, Y., Montcouquiol, M., Zhou, L., Komatsu, K., Shi, D., Fujimori, T., Labeau, J., Tyteca, D., Courtoy, P. et al. (2010). Lack of cadherins Celsr2 and Celsr3 impairs ependymal ciliogenesis, leading to fatal hydrocephalus. *Nat. Neurosci.* **13**, U700-U71. doi:10.1038/nn.2555

Toya, M. and Takeichi, M. (2016). Organization of non-centrosomal microtubules in epithelial cells. *Cell Struct. Funct.* **41**, 127-135. doi:10.1247/csf.16015

Toya, M., Kobayashi, S., Kawasaki, M., Shioi, G., Kaneko, M., Ishiuchi, T., Misaki, K., Meng, W. and Takeichi, M. (2016). CAMSAP3 orients the apical-to-basal polarity of microtubule arrays in epithelial cells. *Proc. Natl. Acad. Sci. USA* **113**, 332-337. doi:10.1073/pnas.1520638113

Vladar, E. K., Bayly, R. D., Sangoram, A. M., Scott, M. P. and Axelrod, J. D. (2012). Microtubules enable the planar cell polarity of airway cilia. *Curr. Biol.* **22**, 2203-2212. doi:10.1016/j.cub.2012.09.046

Werner, M. E., Hwang, P., Huisman, F., Taborek, P., Yu, C. C. and Mitchell, B. J. (2011). Actin and microtubules drive differential aspects of planar cell polarity in multi-ciliated cells. *J. Cell Biol.* **195**, 19-26. doi:10.1083/jcb.201106110

Yang, Y. and Mlodzik, M. (2015). Wnt-Frizzled/planar cell polarity signaling: cellular orientation by facing the wind (Wnt). *Annu. Rev. Cell Dev. Biol.* **31**, 623-646. doi:10.1146/annurev-cellbio-100814-125315

Yuba-Kubo, A., Kubo, A., Hata, M. and Tsukita, S. (2005). Gene knockout analysis of two gamma-tubulin isoforms in mice. *Dev. Biol.* **282**, 361-373. doi:10.1016/j.ydbio.2005.03.031

Zar, J. H. (2010). *Biostatistical Analysis*, 5th edn. London: Pearson Education International.